Bio-interactions and Biocompatibility

Foreign Body Reaction to a Subcutaneously Implanted Self-Cleaning, Thermoresponsive Hydrogel Membrane for Glucose Biosensors

Alexander A. Abraham, Anna Kristen Means, Fred J. Clubb, Ruochong Fei, Andrea K. Locke, Erica G. Gacasan, Gerard L Cote, and Melissa A. Grunlan

ACS Biomater. Sci. Eng., **Just Accepted Manuscript** • DOI: 10.1021/acsbiomaterials.8b01061 • Publication Date (Web): 09 Oct 2018

Foreign Body Reaction to a Subcutaneously Implanted Self-Cleaning, Thermoresponsive Hydrogel Membrane for Glucose Biosensors

*Alexander A. Abraham,[1]‡ A. Kristen Means,[2]‡ Fred J. Clubb, Jr., [1,3] Ruochong Fei,[1] Andrea K. Locke,[1] Erica G. Gacasan,[1] Gerard L. Coté,[1,4] and Melissa A. Grunlan[1,2,4]**

[1]Department of Biomedical Engineering, Texas A&M University, College Station, TX 77843-2120 (USA)

[2]Department of Materials Science & Engineering, Texas A&M University, College Station, TX 77843 (USA)

[3]Department of Veterinary Pathobiology, Texas A&M University, College Station, Texas 77843-4467 (USA)

[4]Center for Remote Health Technologies and Systems, Texas A&M University, College Station, TX 77843-3577 (USA)

**Corresponding Author*:
Prof. M.A. Grunlan
Tel: 01 979 845 2406
Fax: 01 979 845 4450
Email: mgrunlan@tamu.edu

Keywords: biocompatibility, thermoresponsive, hydrogel, PNIPAAm, double network

Abstract

Towards achieveing a subcutaneously implanted glucose biosensor with long-term functionality, a thermoresponsive membrane previously shown to have potential to house a glucose sensing assay was evaluated herein for its ability to minimize the foriegn body reaction (FBR) and the resulting fibrous capsule. The severity of the FBR proportionally reduces diffusion of glucose to the sensor and hence sensor lifetime. However, efforts to reduce the FBR have largedly focused on anti-fouling materials that passively inhibit cellular attachment, particularly poly(ethylene glycol) (PEG). Herein, the extent of the FBR of a subcutaneously implanted "self-cleaning" cylindrical membrane was analyzed in rodents. This membrane represents an "actively anti-fouling" approach to reduce cellular adhesion. It is a thermoresponsive double network nanocomposite hydrogel (DNNC) comprised of poly(*N*-isopropylacrylamide) (PNIPAAm) and embedded polysiloxane nanoparticles. The membrane's cyclical deswelling/reswelling response to local body temperature fluctuations was anticipated to limit cellular accumulation. Indeed, after 30 days, the self-cleaning membrane exhibited a notably thin fibrous capsule (~30 μm) and increased microvascular density within 1 mm of the implant surface in comparison to a non-thermoresponsive, benchmark biocompatible control (PEG diacrylate, PEG-DA).

Introduction

Thermoresponsive poly(*N*-isopropylacrylamide) (PNIPAAm) hydrogels undergo cyclical deswelling and reswelling at temperatures above and below, respectively, their volume phase transition temperature (VPTT).[1-6] This dynamic nature of PNIPAAm has been utilized in various biomedical applications such as drug delivery[7-8] and cell sheet engineering[6, 9]. We hypothesized that this mechanism could be used by membranes surrounding subcutaneously implanted glucose biosensors to control biofouling, a leading cause of device failure. Specifically, such a thermoresponsive membrane could house a liquid glucose sensing assay[10] as an electronics-free, subcutanteously implantable glucose biosensor that could be accompanied with a wearable, optical detection method. Previously, we reported a glucose biosensor membrane candidate, a thermoresponsive double network nanocomposite (DNNC) hydrogel composed of an interpenetrating, asymmetrically cross-linked PNIPAAm matrix with polysiloxane nanoparticles (~200 nm diameter) embedded during the formation of the 1st network.[11] Cyclical deswelling/reswelling with heating/cooling around its VPTT was shown to effectively cause the detachment of cultured cells. Furthermore, this membrane did not limit glucose diffusion (D ~2.7x10^{-6} cm^{2}s^{-1})[12] and also provided robust mechanical strength (strength ~0.4 MPa)[11] versus conventional hydrogels (~1-100s kPa)[13] necessary for long-term durability. Moreover, its modulus (E ~0.2 MPa)[11] remained similar to that of the native subcutaneous and dermis tissues (E ~0.01-0.25 MPa)[14-16], avoiding adverse shear stresses often experienced by tissues surrounding current metallic, transdermal CGM electrodes.[17] However, the ability of this thermoresponsive DNNC membrane to limit the foreign body reaction (FBR) has yet to be established and represents a primary challenge in the development of subcutaneously implanted glucose and other biosensors that possess lifetimes of months rather than only days. For an

implanted biosensor to remain functional long-term, sufficient diffusion of the analyte (e.g. glucose) to the sensor must be maintained throughout the initial (acute) host response, FBR and healing processes that are triggered by implantation. The FBR particularly leads to the formation of a dense, avascular fibrous capsule comprised of fibroblasts, fibrocytes and collagenous tissue.[18] Depending on the extent of the FBR, this compact fibrous capsule may vary from 30 to >200 μm in thickness and may lack nearby vascularization, thereby limiting analyte diffusion.[19-22] Moreover, the FBR and resulting fibrous capsule, once formed, remain present for the lifespan of the implanted device.[18] Therefore, to ensure analyte diffusion to the biosensor, measures must be taken to minimize the FBR as well as to encourage healing so as to reduce the formation of this dense tissue barrier and increase nearby microvascularization.

After the subcutaneous implantation of a membrane-coated glucose biosensor or other device, a series of sequential, innate host responses occur, including: injury, humeral interactions (proteins, complements, kinins, etc.), acute inflammatory response, chronic inflammatory response, FBR, granulation tissue formation (admixture of lymphocytes, macrophages, fibroblast and neovascular buds) and fibrous capsule formation.[23] Acute inflammation, chronic inflammation and FBR are often investigated in tandem as these stages are closely related and provide insight into the host response to a biomaterial.[23] The acute inflammatory response is primarily impacted by local damage to the surrounding tissue where a greater implantation trauma will result in a more amplified acute response.[18] Therefore, minimizing injury during implantation is essential. In the case of subcutaneous biosensors, this can be accomplished with injection, but does limit the implant‘s geometry and size. Additionally, the chemical and physical properties of the implant can potentially lead to chronic inflammation and a heightened FBR. In order to minimize the FBR, numerous groups have concentrated on “passively anti-fouling”

polymeric materials that reduce protein and cellular adhesion, including: poly(tetrafluoro-ethylene) (PTFE),[19, 24-26] poly(vinyl alcohol) (PVA)[25-26] and poly(ethylene glycol) diacrylate (PEG-DA).[27-29] However, *in vivo* investigations with each of these materials have shown the presence of a fibrous capsule surrounding the implant of up to >100 μm,[19, 24, 26] with PEG-DA exhibiting the thinnest capsule, ~30 μm.[29] Currently, most commercialized transcutaneous continuous glucose monitoring (CGM) sensors (i.e. Dexcom Seven®, Guardian™) use stiff metal electrodes, such as platinum,[30] which have limited lifetimes of days due to the host response.[31] To enhance biocompatibility and lifetime, many transcutaneous electrodes and optical fibers have been coated with non-fouling polymers including Nafion,[32-34] polyurethanes[35-36] and PEG-DA.[28, 37-38] Although transcutaneous CGMs have improved significantly over recent years, the lifetime of these devices remain limited to < ~2 weeks.[31, 39-41]

In contrast to these passively anti-fouling approaches, the thermoresponsive DNNC hydrogel membrane described herein relies on an "actively anti-fouling" or "self-cleaning" approach to physically detach adsorbed cells from its surface and also to limit initial cellular attachment strength and stability.[1-2, 11-12] Having previously confirmed glucose diffusion, mechanical properties, swelling kinetics and cytocompatibility,[11-12] the DNNC membrane's thermally-driven self-cleaning behavior was then demonstrated *in vitro* by the reduction of cellular adhesion and successful cell-release when thermally cycled with an external heating system.[12] In this work, a rodent animal model was utilized to evaluate the extent of the FBR elicited by this self-cleaning membrane in a biological enviroment. Time points of seven and 30 days were utilized as these represent early- and mid-stages of healing. Here, we relied on local body temperature fluctuations around the membrane to drive cell detachmant in contrast to using an external heating source to remove cultured cells. The DNNC hydrogels were prepared as

cylinders (diameter ~1.5 mm, length ~5 mm) and implanted into the dorsal subcutaneous tissue of rats via injection with a trocar needle. This represents a plausbile geometry for a membrane-based glucose biosensor and an implantaion method that minimizes injury. Passively anti-fouling PEG-DA implants were evaluated in parallel to represent a benchmark response as a hydrophilic (Figure S1A), biocompatible control with high dimensional stability (i.e. non-thermoresponsive to the temperature range of the subcutaneous tissue of rats). While the PEG-DA implants exhibited a higher modulus than the DNNC membranes (Figure S1B), their stiffness remained much lower than most metallic CGM electrodes (moduli ~GPa). Thus, the objective of this work is to assess the extent of the FBR around the DNNC membrane implants *in vivo* under normal local body temperature fluctuations without the need for an external transdermal heating system.

Experimental

Materials. *N*-Isopropylacrylamide (NIPAAm, 97%), *N*-vinylpyrrolidone, and poly(ethylene glycol) diacrylate (PEG-DA, MW 575 g/mol) were purchased from Sigma-Aldrich (St. Louis, MO). *N*,*N*'-methylenebisacrylamide (BIS, 99%) was purchased from Acros Organics (Geel, Belgium). 2-Hydroxy-2-methyl-1-phenyl-1-propanone (Darocur 1173) and 1-[4-(2-Hydroxy)-phenyl]-2-hydroxy-2-methyl-1-propane-1-one (Irgacure 2959) was purchased from Ciba Specialty Chemicals (Tarrytown, NY). Octamethylcyclotetrasiloxane (D4) and 1,3,5,7-tetra-methyl-1,3,5,7-tetra¬vinylcyclotetrasiloxane (D4Vi) came from Gelest, Inc. Dodecylbenzene-sulfonic acid (DBSA, BIO-SOFT® S-101) came from Stepan Co. (Northfield, IL). For hydrogel fabrication and other experiments, deionized water (DI) with a resistance of 18 MΩ·cm (Millipore, Billerica, MA) was used.

Polysiloxane Nanoparticle Preparation. Polysiloxane colloidal nanoparticles with an average diameter of ~200 nm were prepared via emulsion polymerization and purified via dialysis as previously reported.[2] The final emulsion was 4.8 wt% solids.

DNNC Hydrogel Preparation. DNNC hydrogels were prepared by sequential formation of a relatively tightly crosslinked 1st network containing polysiloxane nanoparticles (2 wt% solid nanoparticles based on NIPAAm weight) and a loosely crosslinked 2nd network.[11] The "1st network precursor solution" was formed by combining NIPAAm monomer (1.0 g), NVP co-monomer (0.16 g), BIS crosslinker (0.04 g), polysiloxane nanoparticle emulsion (0.485 g), Irgacure-2959 photoinitiator (0.08 g) and DI (6.54 g). The "2nd network precursor solution" was formed by combining NIPAAm (6.0 g), NVP (0.96 g), BIS (0.012 g), Irgacure 2959 (0.24 g), and DI (21.0 g). Cylindrical hydrogels (~1.5 mm x 5 mm, diameter x length) were prepared by pipetting the 1st network precursor solution into a cylindrical glass mold (inside diameter = 1.0 mm, length = 15 mm). The mold was immersed in an ice water bath (~7 °C) and exposed for 10 min to longwave UV light. Cylindrical hydrogels were removed from their molds, rinsed with DI, and soaked in a Petri dish containing DI (60 mL) for 2 days at RT with daily water changes. The cylindrical hydrogels were then transferred into a Petri dish containing the 2nd network precursor solution for 24 hr at RT. Each cylindrical hydrogel was then placed into a second cylindrical mold (diameter = 1.5 mm, length = 15 mm), submerged in an ice water bath (~7 °C), exposed for 10 min to longwave UV light and soaked in DI as above. A clean razor blade was used to trim ends to reduce the cylindrical length to 5 mm. The final diameter was measured via calipers. Similarly, planar sheet hydrogels were formed by injection of the 1st precursor solution between two glass slides separated by 1 mm spacers and UV irradiated for 30 min in an ice water bath (~7 °C). The planar gels were allowed to soak in DI for 2 days and then transferred into the

2nd precursor solution for 2 days. Each planar gel was placed between two glass slides separated by 1 mm spacers, UV irradiated for 30 min in an ice water bath (~7 °C) and soaked in DI as above.

PEG-DA Hydrogel Cylinder Preparation. Precursor solutions were formed by vortexing PEG-DA (100 %v/v) and Darocur 1173 (1% v/v) for 1 min. Cylindrical hydrogels (~1.5 mm x 5 mm, diameter x length per electronic caliper) were prepared by pipetting the precursor solution into a hollow cylindrical glass mold (inside diameter = 1.0 mm, length = 15 mm) with one end sealed by Parafilm. After sealing the other end of the mold, it was exposed to longwave UV light (UV-Transilluminator, 6 mw/cm^2, 365 nm) at room temperature (RT) for 3 sec. The cylindrical hydrogel was removed from the mold, rinsed with DI and immersed in a Petri dish containing DI (60 mL) for 24 hr. A clean razor blade was used to equally trim the ends to reduce the length to 5 mm. Similarly, planar PEG-DA hydrogels were prepared by injecting the precursor solution between two glass slides separated by 1 mm spacers and UV irradiating for 20 sec at RT. The planar gels were removed from the molds and soaked in DI as above.

Implanted DNNC Thermocycling Theoretical Diameter Change. Previously reported DNNC thermosensitivity data [12] was best-fit to a linear function spanning the expected implanted DNNC hydrogel cylinder temperature range (37-38 °C) seen in the subcutaneous tissue due to innate body temperature fluctuations of rats.[42-43] This linear function was then used to determine the theoretical dimensional change with respect to ~1 °C oscillations of the implanted DNNC hydrogel cylinder temperature.

Mesh Size of DNNC Hydrogels. Due to the complex structure of DN hydrogels, the mesh size is unable to be determined through standard calculations that typically require the molecular

weight between crosslinks[44-45] which is difficult to estimate with two interpenetrating, assymetrically crosslinked networks. Thus, in this study, DNNC mesh size was characterized via a series of dextran diffusion experiments, similar to as previously reported.[46] Hydrogel discs (~13 x 1.2 mm, diameter x thickness) were punched from hydrogel sheets and each were soaked in 1 mL of 0.01 mg mL^{-1} concentrated FITC-dextran DI solutions (4, 10, 20, 40, 70, 150 or 250 kDa, 3 discs for each mol. wt.). After 24 h at RT, the hydrogel discs were removed, gently rinsed with DI and blotted dry before transfering to 1 mL of fresh DI on a shaker table at 150 rpm. The dye was allowed to diffuse out of the hydrogels and the fluroescence of the surrounding solution was measured at 0 h and after 24 h at ex/em 480/520 nm. Standard calibration curves for each FITC-dextran size were used to convert fluorescence intensity to concentration. When the difference in concentration from 0 h to 24 h fell to negligible levels, it was assumed that diffusion was inhibited and therefore the mesh size could be correlated to a size range between that of the FITC-dextrans at this point.

Implantation & Histological Evaluation. PEG-DA and DNNC cylindrical hydrogels (diameter ~1.5 mm, length ~5 mm) were sterilized by exposure to 80% ethanol for 45 min. Hydrogels were then washed three times for 30 min with sterile Dulbecco's phosphate buffer solution (PBS). Disposable, sterile trocar needles (13G; inner diameter = 1.804 mm, Avid Identification Systems, Inc.) were utilized to inject a single cylindrical hydrogel into the subcutaneous tissue (2~3 mm in depth) within the panniculus muscle (Figure 1) in the dorsal of CD® Hairless rats (N = 20, male, 8 weeks old, Charles River Laboratories). The CD® Hairless rat species encompasses a normal immune response despite its abnormal, reduced hair growth. The rat's hairless characteristic is ideal to facilitate the membrane implantation without unwarranted skin irritation commonly associated with shaving and nairing. Using isoflurane by inhalation,

animals were anesthetized and anesthesia depth was tested by foot pinch reaction. Following implantation, the injection site was closed with surgical adhesive (3M Vetbond™ Tissue Adhesive, No. 1469SB). Material composition and dorsal placement were recorded for each rat/implant. All animals were immediately returned to individual cages and monitored every 12 hr. A custom designed LabView program (National Instruments) recorded cage temperatures every 5 min. After either 7 or 30 days post-implantation, 10 animals were euthanized by CO_2 asphyxiation, photographed, evaluated for gross changes and immediately fixed in 10% neutral buffered formalin for one week. Finally, implants and their surrounding tissue were removed and processed for histology by serial dehydration, paraffin embedding, sectioning, and staining (hematoxylin and eosin (H&E)).

All morphometric analysis was performed in the Cardiovascular Pathology Laboratory (CVP) in the College of Veterinary Medicine & Biomedical Sciences at Texas A&M University by a board certified pathologist (Dr. Fred Clubb, DVM) that remained blinded throughout the study. Each tissue cross-section was scanned to enable consistent viewing at 100x using OlyVIA Olympus slide-viewing software during analysis to provide a standard field of view (~50 μm x ~70 μm, height x width). Each cross-section was divided into 4 sectors (Figure S2) and 100 cells per sector were identified manually by established morphometric parameters as neutrophils, eosinophils, lymphocytes, erythrophagocytosis, hemosiderin-laden macrophages, macrophages, fibroblasts, fibrocytes, multi-nucleated giant cells (MNGCs) or plasma cells. The percentages of each cell type were calculated for each sector and averaged giving an average cellular presence around each implant type per animal. These values were then averaged over all animals for each implant type to get the final reported percentages at each time point. Additionally, in each sector the presence of capillaries, fibrin, loose collagen and dense collagen was recorded as (-)

indicating little to no presence, (+/-) indicating low presence and (+) indicating high presence. To further evaluate microvascular density, blood vessels (10-100 μm in diameter) within 1 mm of the superficial half of the polymer interface were manually counted. Finally, a healing score was assigned to each sector utilizing a criteria (Table S1) previously established in the CVP lab[47] to determine the healing stage at each time point. Fibrous capsule thickness was measured at 8 distinct locations, 12:00 corresponding to the most superior point of the capsule nearest the dermis and 6:00 corresponding to the most inferior point of the capsule (Figure S2). The depth of the implant was determined from the outermost edge of the dermis to the interface of the hydrogel with the tissue at the 12:00 position. Furthermore, the diameter of each hydrogel cylinder was measured from the 12:00 to 6:00 position (perpendicular to the dermis) and the 3:00 to 9:00 position (parallel to the dermis) as shown in Figure S2. All capsule measurements were performed blinded to avoid potential bias. Multiple student's T-tests with the Holm-Sidak correction were applied to determine significance ($p < 0.05$) in all histological analysis. *IACUC Approval*. NIH guidelines for the care and use of laboratory animals (NIH Publication #85-23 Rev. 1985) have been observed. All animal investigations conducted were approved by the Texas A&M University Institutional Animal Care and Use Committee and fell under the Animal Use Protocol #2012-191.

Results and Discussion

DNNC hydrogel fabrication and characterization. The thermoresponsive DNNC membrane fabrication has been previously described[12] to obtain a cylindrical geometry for ease of implantation via trocar needle. Although these do not contain macropores, all hydrogels inherently have a mesh-like network that can be tuned through factors such as crosslink density and/or monomer concentration, thereby tailoring diffusion rates and swelling properties. Due to

the multi-network design of these DNNC membranes, the traditional models used to calculate mesh size from equilibrium swelling ratios[44-45] could not be easily adopted. Therefore, in this study a size exclusion experiment was performed via diffusion of varying sizes of FITC-dextran (4, 10, 20, 40, 70, 150, and 250 kDa MW) to estimate the mesh size. The mesh size of the DNNC hydrogels at RT was determined to be between 6.5 and 9.6 nm (Figure S3), corresponding to the hydrodynamic diameters (D_h) of 20 and 40 kDa FITC-dextran respectively.[48] As a result, glucose (D_h ~1 nm) would be expected to diffuse freely through this membrane, with a diffusion coefficient of 2.73 ± 0.01x10^{-6} cm^2s^{-1} (at RT) and 1.88 ± 0.001 (at 35 °C) as was reported previously.[12] This nicely matches the diffusion coefficient of the surrounding dermis tissue, reported as 2.64 ± 0.42x10^{-6} cm^2s^{-1}.[49] With their comparable glucose diffusivity, the DNNC hydrogels show great potential as self-cleaning, biosensor membranes that would not severely limit analyte diffusion.

Deswelling/reswelling behavior of thermoresponsive DNNC hydrogel cylinder. By undergoing cyclical deswelling/reswelling, implanted thermoresponsive membranes were expected to actively inhibit cellular attachment and/or facilitate cellular detachment, and so potentially reduce the severity of the FBR. The core body temperature oscillations in normal male rats have been reported in literature to range from ~37.0-38.0 °C over a 24 hr period.[42-43] Additionally, studies comparing body temperatures measured rectally (core) to temperatures measured by subcutaneously implanted monitors have confirmed that the core body temperature of rats is approximately equal to that of the subcutaneous tissue.[50] However, the VPTT of conventional crosslinked PNIPAAm hydrogels is ~33-35 °C and would so render such an implanted membrane in a fully deswollen, "static" state not conducive for cell-release or for maximum glucose diffusivity. Thus, the VPTT of the DNNC hydrogel was tuned to 36.5

°C (onset temperature, T_o) and 39.5 °C (maximum temperature,T_{max}) by incorporation of a hydrophilic comonomer (NVP).[12] Previously reported DNNC thermosensitivity data[12] was best-fit to a linear function spanning the expected implanted DNNC hydrogel cylinder temperature range (37-38 °C) to quantify the corresponding diameter change. The theoretical maximum diameter change of a cylindrical hydrogel (~1.5 mm x 5 mm, diameter x length) over this estimated 1.0 °C temperature oscillation from 37 to 38 °C was calculated to be ~9 μm. During a 24 hr period, the DNNC hydrogel cylinder would undergo constant dimensional alterations while still remaining in a hydrated, swollen state well below its VPTT (T_{max} = 39.5 ºC) but slightly over the onset temperature of the transition (T_o = 36.5 ºC).[12] This consistent, localized change at the implant-tissue interface could potentially decrease cell adhesion on the DNNC surface, inhibiting the formation of a dense fibrous capsule around the biosensor. For the non-thermoresponsive PEG-DA implant, it was previously shown to exhibit dimensional stability over a broad range of temperatures (25-40 ºC).[12]

Implantation of PEG-DA and self-cleaning DNNC hydrogel implants. Using a trocar needle, one sterile cylindrical (diameters ~1.5 mm, length ~5 mm) thermoresponsive DNNC hydrogel and one PEG-DA (non-thermoresponsive control) were implanted into the dorsal panniculus muscle (1~3 mm in depth, Figure 1, Figure S4A) lateral to the spine of CD® Hairless rats (N = 20, male, 8 weeks old). This location was chosen for the higher vascular density compared to that of the adipose tissue of the subcutaneous region.[51] A greater amount of vascularization is desired to reduce the lag time between blood glucose to interstitial glucose levels in the tissue surrounding the biosensor membrane. One potential drawback of implanting into a more vascularized tissue is the greater initial injury imparted by the trocar needle, which may lead to a more intense acute inflammatory response. However, by evaluating the cellular

response at 7 and 30 days, we were able to determine the extent of acute inflammation after 1 week and to monitor its resolution over time to ensure that proper healing was achieved. At each time point after explantation, the implant diameters of both implant types remained similar to the original implant geometry (diameters ~1.5 mm, Figure S4B).

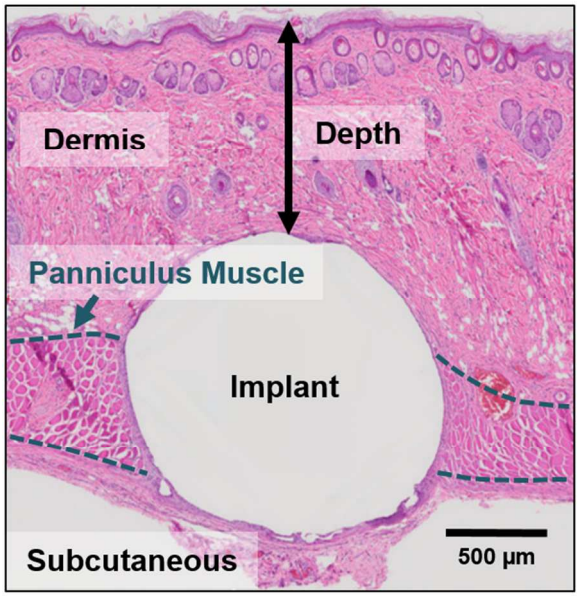

Figure 1. Representative histological image of cylindrical hydrogel implant cross-section, showing the location of implantation within the panniculus muscle and the typical depth (~1-3 mm).

Cellular response. To evaluate the host response induced by the thermoresponsive DNNC membranes, the presence of dominant cellular components related to inflammation and healing was determined at 7 and 30 days to investigate the early- and mid-stages of healing (Figure S5). As a benchmark biocompatible material, dimensionally stable PEG-DA was utilized as a positive control to establish a favorable cellular response. During early-healing (~3-10 days), the acute inflammation caused by the minimal trauma incurring from implantation should begin to recede. At 7 days, cellular presence around both material compositions consisted mainly

of macrophages with small numbers of fibroblasts, lymphocytes, neutrophils and multi-nucleated giant cells (MNGCs), as shown in Figure 2. Macrophages are strongly recruited to the site of injury during acute inflammation;[52-53] therefore, this result was expected. Notably, a slightly lower amount of macrophages was present surrounding the thermoresponsive DNNC membrane compared to the PEG-DA implant. We hypothesize that the lower modulus (Figure S1B), similar to that of the surrounding tissue, as well as the dimensional instability of the self-cleaning membranes produced a slightly milder acute inflammatory response. The clearing of red blood cells generated from vascular injury is confirmed by the reduction in erythrophagocytosis seen from 7 to 30 days (Figure S6). Furthermore, the number of inflammatory cells, including macrophages and MNGCs, were seen to significantly decrease at the 30 day time point, indicating resolution of the acute inflammatory response into mid-stage healing. Additionally, the presence of fibroblasts and fibrocytes increased after 30 days, indicating the formation of fibrous capsule tissue and a typical healing response. From the types of cells observed and the notable progression towards healing, the DNNC membranes demonstrated high biocompatibility and did not elicit any substantial adverse reactions by the body.

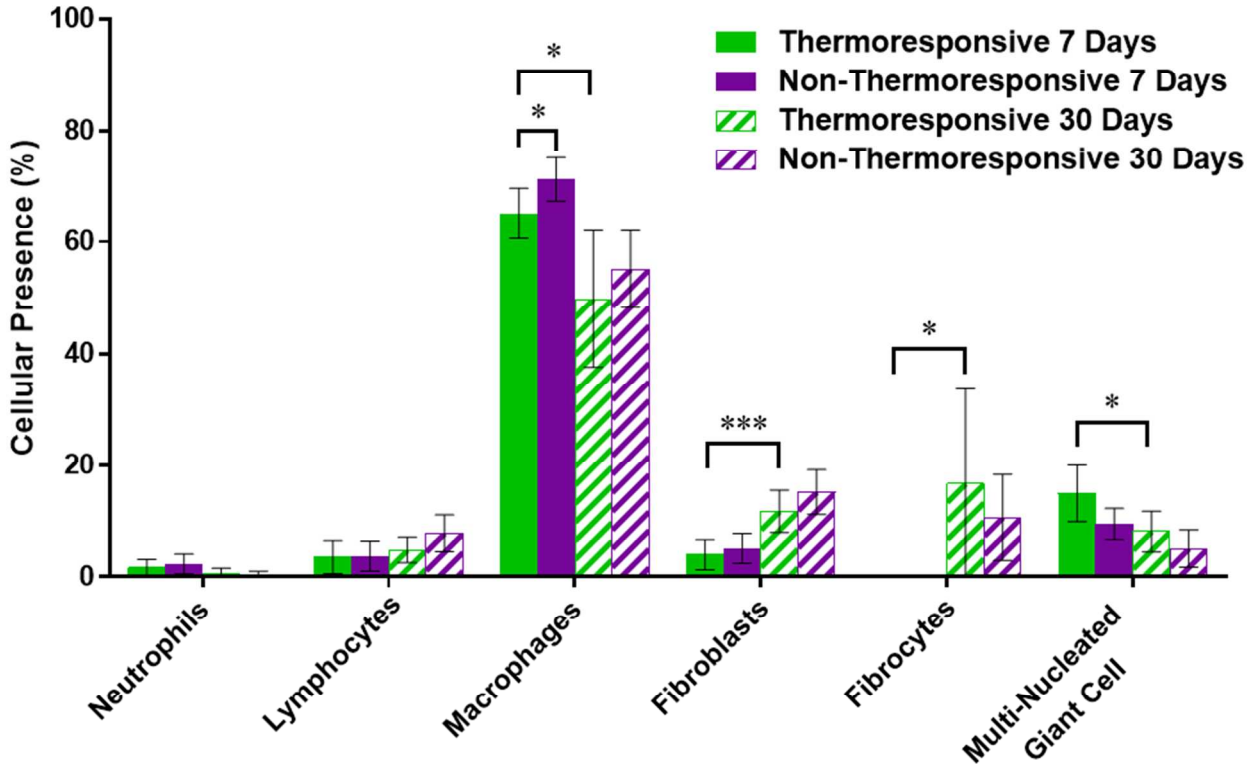

Figure 2. Cellular response surrounding thermoresponsive DNNC and non-thremoresponsive PEG-DA implants. Graphical analysis displaying the various cell types and their approximate percentage adjacent to DNNC and PEG-DA implants after 7 (solid) and 30 days (striped), where * indicates a significant difference of $p < 0.05$ and *** indicates a significant difference of $p < 0.005$.

Fibrous capsule formation. The formation of a dense avascular fibrous capsule around the biosensor will inhibit the rate of glucose diffusion from the surrounding interstitial fluid. This reduction in rate can be directly correlated with the thickness of the capsule (i.e. increased thickness, increased sensor lag time). Fibrosis occurs in the later stages of the FBR (weeks rather than days).[54] Thus, at 7 days the tissue capsule around the implant was an unorganized cellular layer without significant fibrous tissue. The width of this unorganized cellular tissue surrounding the thermoresponsive DNNC was measured at multiple points (Figure S2) that resulted in 37.5 ±

11.0 μm (Figure 3) across all animals. The high deviation in the measured thickness at 7 days could be explained by the high cellularity resulting in a poorly defined tissue capsule. However, as resolution proceeded for 30 days, the capsule around the DNNC implants became more fibrous and well-defined. This organized, collagenous tissue capsule exhibited an average thickness of 33.2 ± 6.1 μm, nearing the minimum thickness typically reported in literature, ~30 μm.[19-22] and slightly thinner than the passively anti-fouling PEG-DA control with a thickness of 45.9 ± 13.4 μm (Figure 3). By inhibiting the fibrous capsule formation, this self-cleaning membrane may reduce sensor lag time in a potential implantable biosensor.

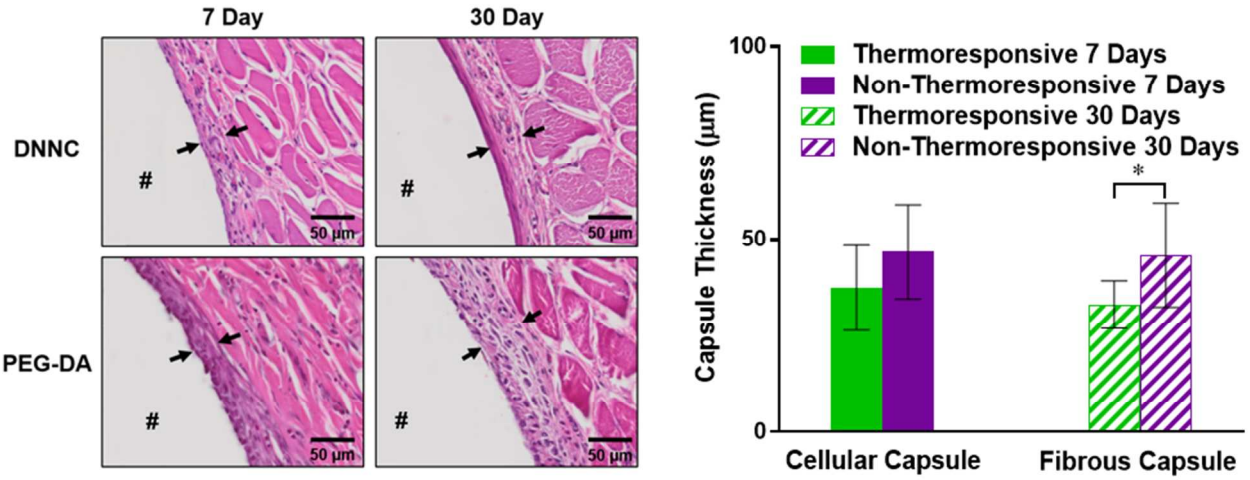

Figure 3. Representative histological images showing the cross-section of the thermoresponsive DNNC (top) and non-thermoresponsive PEG-DA (bottom) implants indicated by (#) and the surrounding tissue at 7 and 30 days, highlighting the fibrous capsule thickness indicated by the double arrows. The graph shows the quantitative tissue capsule thickness surrounding the thermoresponsive and non-thermoresponsive membranes at 7 days (solid, cellular capsule) and 30 days (striped, fibrous capsule), where * indicates a significant difference of $p < 0.05$ and *** indicates a significant difference of $p < 0.005$.

Additionally, the composition of the capsule around the implant is important in determining the extent of healing. Thus, the fibrotic tissue presence, including fibrin and collagen, was evaluated qualitatively over 7 and 30 day time points with (-) indicating little to no presence, (+/-) indicating low presence and (+) indicating high presence (Table S2). Fibrin is released from the blood during initial injury, thus is more prevalent at the earlier time point of 7 days. Activated fibroblasts produce collagen, which densifies as healing matures. Due to the relatively low number of fibroblasts seen near the implants at 7 days (Figure 2), only small regions of loose collagen were found at this time point. With the recruitment of more fibroblasts at 30 days, an increase in loose collagen was observed as well as trace amounts of dense collagen. This progression from loose fibrin to a dense collagenous capsule demonstrates normal resolution during the FBR.

Although a dense fibrous capsule indicates appropriate healing, it can potentially inhibit glucose diffusion to the biosensor. Therefore, microvascular presence within the capsular tissue is important to carry glucose closer to the implant surface. Around both implant types, as expected due to a lack of macroporosity, a greater amount of vascularization was found in the outer regions of the tissue capsule than in the tissue nearest the implant surface (Table S2). To quantify microvascular presence, blood vessels (10-100 μm in diameter) within 1 mm of the superficial half of the hydrogel interface were counted. It was determined that DNNC hydrogels had a significantly higher vascular density (vessels per mm^2) than the benchmark biocompatible PEG-DA implants post 30 days (Figure 4). We hypothesize that the dynamic nature at the DNNC hydrogel surface may promote a less organized extracellular matrix and promote neovascularization.

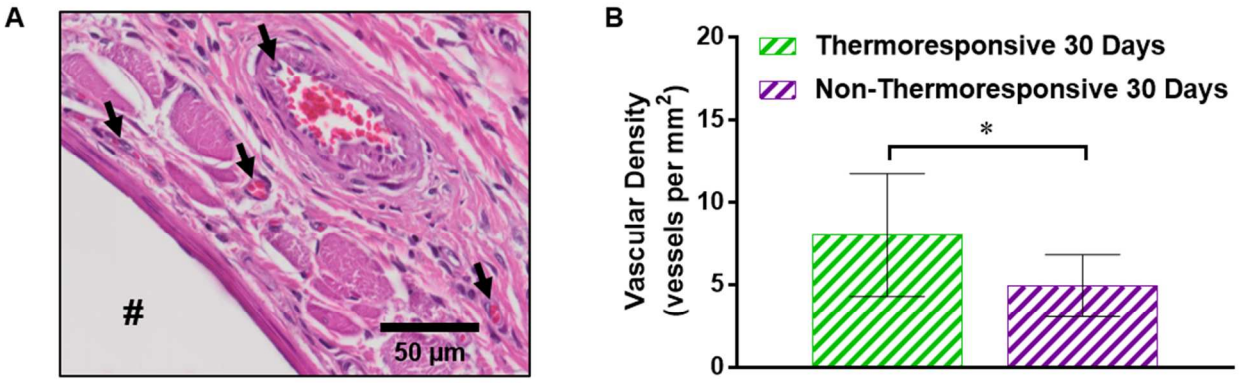

Figure 4. A) Representative histological image showing the cross-section of a thermoresponsive DNNC implant indicated by (#) and the surrounding tissue at 30 days, highlighting the microvasculature presence indicated by arrows. B) The average vascular density within 1 mm of the implants after 30 days of implantation. For statistics, * indicates a significant difference of $p < 0.05$.

As an overall confirmation of proper resolution around the implants, the dominant substrate and cellular components were evaluated and compiled into a healing score, rated from 0 to 6 from initial implantation to end-stage healing as defined in Table S1. This criteria used for determining the stage of healing has been well established by the Cardiovascular Pathology Laboratory. In Figure S7, the expected progression of healing from early-stage at 7 days to mid-stage at 30 days was confirmed for the DNNC implants.

Conclusion

Towards establishing its utility to house a subcutaneous glucose biosensor with long-term functionality, the biocompatibility of a thermoresponsive DNNC hydrogel membrane was evaluated in a rodent model in terms of its ability to minimize the FBR. This membrane was previously shown to effectively release culture cells with thermal cycling around its VPTT.

Herein, the implanted membrane relied on an "actively anti-fouling" or "self-cleaning" mechanism to limit cell adhesion and the subsequent FBR. Having tuned its VPTT (**T_o** = 36.5 °C; T_{max} = 39.5 °C)**,** the implanted cylindrical membrane (diameter ~1.5 mm, length ~5 mm) was expected to remain in a largely swollen state but undergo small diameter changes (~9 μm) due to normal body temperature fluctuations (~37-38 °C). DNNC hydrogel cylinders were implanted subcutaneously (via injection) for 7 and 30 days to observe the FBR at both early- and mid-stages of healing, respectively. "Passively anti-fouling" PEG-DA implants were evaluated in parallel as a non-thermoresponsive, benchmark biocompatible control. Notably, after 30 days, the fibrous capsule surrounding the thermoresponsive membranes was remarkably thin (~33 μm) versus those typically reported in literature (~30 to >100 μm) and slightly thinner than that of the passively anti-fouling PEG-DA implants (~46 μm). Moreover, the microvascular density around the DNNC implant was greater than that surrounding the non-thermoresponsive PEG-DA. By minimizing the fibrous capsule thickness and enhancing local vascularization, the self-cleaning DNNC membrane provides a potential solution to avoid reductions in analyte (glucose) diffusion to implanted biosensors. By utilizing an actively anti-fouling or self-cleaning approach rather than a passively anti-fouling approach, the DNNC membranes demonstrate an alternative method to control the FBR through constant dimensional change at the implant surface inhibiting cell accumulation and stability. Overall, the thermoresponsive DNNC membrane's high biocompatibility combined with previously established *in vitro* properties (e.g. glucose diffusion and mechanical strength), make it a desirable candidate for a long-term, implantable glucose biosensor.

ASSOCIATED CONTENT

Supporting Information.

The following files are available free of charge.

SupportingInformation_DNNC_ACSBiomatSci&Engr (PDF)

AUTHOR INFORMATION

Author Contributions

The manuscript was written through contributions of all authors. All authors have given approval to the final version of the manuscript. ǂThese authors contributed equally.

Funding Sources

Funding from the NIH/NIDDK (1R01DK095101-01A1) is gratefully acknowledged. This work was supported, in part, by funding from the National Science Foundation Engineering Research Center for Precise Advanced Technologies and Health Systems for Underserved Populations (PATHS-UP) (Award No. 1648451). A.K.M. thanks the NSF Graduate Research Fellowship Program (NSF GRFP M1703014).

Acknowledgements

Funding from the NIH/NIDDK (1R01DK095101-01A1) is gratefully acknowledged. This work was supported, in part, by funding from the National Science Foundation (NSF) Engineering Research Center for Precise Advanced Technologies and Health Systems for Underserved Populations (PATHS-UP) (Award No. 1648451). A.K.M. thanks the NSF Graduate Research Fellowship Program (NSF GRFP M1703014).

References

(1) Gant, R. M.; Hou, Y.; Grunlan, M. A.; Cote, G. L., Development of a self-cleaning sensor membrane for implantable biosensors. *J Biomed Mater Res A* **2009,** *90* (3), 695-701, DOI: 10.1002/jbm.a.32135.
(2) Hou, Y.; Matthews, A. R.; Smitherman, A. M.; Bulick, A. S.; Hahn, M. S.; Hou, H.; Han, A.; Grunlan, M. A., Thermoresponsive nanocomposite hydrogels with cell-releasing behavior. *Biomaterials* **2008,** *29* (22), 3175-84, DOI: 10.1016/j.biomaterials.2008.04.024.
(3) Kobayashi, J.; Okano, T., Fabrication of a thermoresponsive cell culture dish: a key technology for cell sheet tissue engineering. *Sci Technol Adv Mater* **2010,** *11* (1), 014111, DOI: 10.1088/1468-6996/11/1/014111.
(4) Okano, T.; Yamada, N.; Okuhara, M.; Sakai, H.; Sakurai, Y., Mechanism of cell detachment from temperature-modulated, hydrophilic-hydrophobic polymer surfaces. *Biomaterials* **1995,** *16* (4), 297-303, DOI: 10.1016/0142-9612(95)93257-E.
(5) Tang, Z.; Akiyama, Y.; Okano, T., Temperature-responsive polymer modified surface for cell sheet engineering. *Polymers* **2012,** *4* (3), 1478-1498, DOI: 10.3390/polym4031478.
(6) Yang, J.; Yamato, M.; Nishida, K.; Ohki, T.; Kanzaki, M.; Sekine, H.; Shimizu, T.; Okano, T., Cell delivery in regenerative medicine: the cell sheet engineering approach. *J Control Release* **2006,** *116* (2), 193-203, DOI: 10.1016/j.jconrel.2006.06.022.
(7) Dong, L.-C.; Hoffman, A. S., Synthesis and application of thermally reversible heterogels for drug delivery. *J. Controlled Release* **1990,** *13* (1), 21-31, DOI: 10.1016/0168-3659(90)90071-Z.
(8) Qiu, Y.; Park, K., Environment-sensitive hydrogels for drug delivery. *Adv. Drug Delivery Rev.* **2001,** *53* (3), 321-339, DOI: 10.1016/S0169-409X(01)00203-4.
(9) Yamato, M.; Akiyama, Y.; Kobayashi, J.; Yang, J.; Kikuchi, A.; Okano, T., Temperature-responsive cell culture surfaces for regenerative medicine with cell sheet engineering. *Prog. Polym. Sci.* **2007,** *32* (8), 1123-1133, DOI: 10.1016/j.progpolymsci.2007.06.002.
(10) Cummins, B. M.; Li, M.; Locke, A. K.; Birch, D. J. S.; Vigh, G.; Coté, G. L., Overcoming the aggregation problem: A new type of fluorescent ligand for ConA-based glucose sensing. *Biosens Bioelectron* **2015,** *63*, 53-60, DOI: 10.1016/j.bios.2014.07.015.
(11) Fei, R.; George, J. T.; Park, J.; Grunlan, M. A., Thermoresponsive nanocomposite double network hydrogels. *Soft Matter* **2012,** *8* (2), 481-487, DOI: 10.1039/C1SM06105D.
(12) Abraham, A. A.; Fei, R.; Cote, G. L.; Grunlan, M. A., Self-cleaning membrane to extend the lifetime of an implanted glucose biosensor. *ACS Appl Mater Interfaces* **2013,** *5* (24), 12832-8, DOI: 10.1021/am4040653.
(13) Gong, J. P.; Katsuyama, Y.; Kurokawa, T.; Osada, Y., Double-network hydrogels with extremely high mechanical strength. *Adv. Mater.* **2003,** *15* (14), 1155-1158, DOI: 10.1002/adma.200304907
(14) Pailler-Mattei, C.; Bec, S.; Zahouani, H., *In vivo* measurements of the elastic mechanical properties of human skin by indentation tests. *Med Eng Phys* **2008,** *30* (5), 599-606, DOI: 10.1016/j.medengphy.2007.06.011.
(15) Liang, X.; Boppart, S. A., Biomechanical properties of *in vivo* human skin from dynamic optical coherence elastography. *IEEE Trans Biomed Eng* **2010,** *57* (4), 953-959, DOI: 10.1109/TBME.2009.2033464.
(16) Li, C.; Guan, G.; Reif, R.; Huang, Z.; Wang, R. K., Determining elastic properties of skin by measuring surface waves from an impulse mechanical stimulus using phase-sensitive optical coherence tomography. *J R Soc Interface* **2012,** *9* (70), 831-841, DOI: 10.1098/rsif.2011.0583.

(17) Helton, K. L.; Ratner, B. D.; Wisniewski, N. A., Biomechanics of the sensor-tissue interface—effects of motion, pressure, and design on sensor performance and foreign body response—part II: Examples and application. *J Diabetes Sci Technol* **2011,** *5* (3), 647-656, DOI: 10.1177/193229681100500318.
(18) Voskerician, G.; Anderson, J. M., Foreign body reaction. In *Wiley Encyclopedia of Biomedical Engineering*, John Wiley & Sons, Inc.: 2006, DOI: 10.1002/9780471740360.ebs1493.
(19) Bota, P. C.; Collie, A. M.; Puolakkainen, P.; Vernon, R. B.; Sage, E. H.; Ratner, B. D.; Stayton, P. S., Biomaterial topography alters healing *in vivo* and monocyte/macrophage activation *in vitro*. *J Biomed Mater Res A* **2010,** *95* (2), 649-57, DOI: 10.1002/jbm.a.32893.
(20) Morais, J. M.; Papadimitrakopoulos, F.; Burgess, D. J., Biomaterials/tissue interactions: possible solutions to overcome foreign body response. *The AAPS journal* **2010,** *12* (2), 188-96, DOI: 10.1208/s12248-010-9175-3.
(21) Ratner, B. D.; Bryant, S. J., Biomaterials: Where we have been and where we are going. *Annu Rev Biomed Eng* **2004,** *6* (1), 41-75, DOI: 10.1146/annurev.bioeng.6.040803.140027.
(22) Novak, M. T.; Yuan, F.; Reichert, W. M., Modeling the relative impact of capsular tissue effects on implanted glucose sensor time lag and signal attenuation. *Anal Bioanal Chem* **2010,** *398* (4), 1695-1705, DOI: 10.1007/s00216-010-4097-6.
(23) Anderson, J. M.; Rodriguez, A.; Chang, D. T., Foreign body reaction to biomaterials. *Seminars in immunology* **2008,** *20* (2), 86-100, DOI: 10.1016/j.smim.2007.11.004.
(24) Brauker, J. H.; Carr-Brendel, V. E.; Martinson, L. A.; Crudele, J.; Johnston, W. D.; Johnson, R. C., Neovascularization of synthetic membranes directed by membrane microarchitecture. *J Biomed Mater Res* **1995,** *29* (12), 1517-24, DOI: 10.1002/jbm.820291208.
(25) Sharkawy, A. A.; Klitzman, B.; Truskey, G. A.; Reichert, W. M., Engineering the tissue which encapsulates subcutaneous implants. II. Plasma–tissue exchange properties. *J Biomed Mater Res* **1998,** *40* (4), 586-597, DOI: 10.1002/(SICI)1097-4636(19980615)40:4<586::AID-JBM10>3.0.CO;2-E.
(26) Ward, W. K.; Slobodzian, E. P.; Tiekotter, K. L.; Wood, M. D., The effect of microgeometry, implant thickness and polyurethane chemistry on the foreign body response to subcutaneous implants. *Biomaterials* **2002,** *23* (21), 4185-92, DOI: 10.1016/S0142-9612(02)00160-6.
(27) Lynn, A. D.; Kyriakides, T. R.; Bryant, S. J., Characterization of the *in vitro* macrophage response and *in vivo* host response to poly(ethylene glycol)-based hydrogels. *J Biomed Mater Res A* **2010,** *93* (3), 941-53, DOI: 10.1002/jbm.a.32595.
(28) Quinn, C. A.; Connor, R. E.; Heller, A., Biocompatible, glucose-permeable hydrogel for in situ coating of implantable biosensors. *Biomaterials* **1997,** *18* (24), 1665-70, DOI: S0142-9612(97)00125-7.
(29) Swartzlander, M. D.; Lynn, A. D.; Blakney, A. K.; Kyriakides, T. R.; Bryant, S. J., Understanding the host response to cell-laden poly(ethylene glycol)-based hydrogels. *Biomaterials* **2013,** *34* (4), 952-64, DOI: 10.1016/j.biomaterials.2012.10.037.
(30) Vashist, S. K.; Zheng, D.; Al-Rubeaan, K.; Luong, J. H. T.; Sheu, F.-S., Technology behind commercial devices for blood glucose monitoring in diabetes management: A review. *Anal Chim Acta* **2011,** *703* (2), 124-136, DOI: 10.1016/j.aca.2011.07.024.
(31) Nichols, S. P.; Koh, A.; Storm, W. L.; Shin, J. H.; Schoenfisch, M. H., Biocompatible materials for continuous glucose monitoring devices. *Chem Rev* **2013,** *113* (4), 2528-2549, DOI: 10.1021/cr300387j.

(32) Turner, R. F. B.; Harrison, D. J.; Rojotte, R. V., Preliminary *in vivo* biocompatibility studies on perfluorosulphonic acid polymer membranes for biosensor applications. *Biomaterials* **1991,** *12* (4), 361-368, DOI: 10.1016/0142-9612(91)90003-S.
(33) Galeska, I.; Chattopadhyay, D.; Moussy, F.; Papadimitrakopoulos, F., Calcification-resistant nafion/Fe3+ assemblies for implantable biosensors. *Biomacromolecules* **2000,** *1* (2), 202-207, DOI: 10.1021/bm0002813.
(34) Moussy, F.; Harrison, D. J.; O'Brien, D. W.; Rajotte, R. V., Performance of subcutaneously implanted needle-type glucose sensors employing a novel trilayer coating. *Anal Chem* **1993,** *65* (15), 2072-2077, DOI: 10.1021/ac00063a023.
(35) Hu, Y.; Zhang, Y.; Wilson, G. S., A needle-type enzyme-based lactate sensor for *in vivo* monitoring. *Anal Chim Acta* **1993,** *281* (3), 503-511, DOI: 10.1016/0003-2670(93)85008-8.
(36) Yu, B.; Long, N.; Moussy, Y.; Moussy, F., A long-term flexible minimally-invasive implantable glucose biosensor based on an epoxy-enhanced polyurethane membrane. *Biosens Bioelectron* **2006,** *21* (12), 2275-2282, DOI: 10.1016/j.bios.2005.11.002.
(37) Liao, K.-C.; Hogen-Esch, T.; Richmond, F. J.; Marcu, L.; Loeb, G. E. In *Design and fabrication of disposable percutaneous chemical sensors*, SPIE, 2005; pp 129-145, DOI: 10.1117/12.587668.
(38) Sung, W. J.; Na, K.; Bae, Y. H., Biocompatibility and interference eliminating property of pullulan acetate/polyethylene glycol/heparin membrane for the outer layer of an amperometric glucose sensor. *Sens Actuators B Chem* **2004,** *99* (2), 393-398, DOI: 10.1016/j.snb.2003.12.005.
(39) Chen, C.; Zhao, X.-L.; Li, Z.-H.; Zhu, Z.-G.; Qian, S.-H.; Flewitt, A. J., Current and emerging technology for continuous glucose monitoring. *Sensors (Basel, Switzerland)* **2017,** *17* (1), 182, DOI: 10.3390/s17010182.
(40) Klonoff, D. C.; Ahn, D.; Drincic, A., Continuous glucose monitoring: A review of the technology and clinical use. *Diabetes Res Clin Pract* **2017,** *133*, 178-192, DOI: 10.1016/j.diabres.2017.08.005.
(41) Bode, B. W.; Battelino, T., Continuous glucose monitoring. *Int J Clin Pract* **2010,** *64* (s166), 11-15, DOI: doi:10.1111/j.1742-1241.2009.02272.x.
(42) Bolles, R. C.; Duncan, P. M., Daily course of activity and subcutaneous body temperature in hungry and thirsty rats. *Physiol Behav* **1969,** *4* (1), 87-89, DOI: 10.1016/0031-9384(69)90018-3.
(43) Shido, O.; Sakurada, S.; Kohda, W.; Nagasaka, T., Day—Night changes of body temperature and feeding activity in heat-acclimated rats. *Physiol Behav* **1994,** *55* (5), 935-939, DOI: 10.1016/0031-9384(94)90082-5.
(44) Canal, T.; Peppas, N. A., Correlation between mesh size and equilibrium degree of swelling of polymeric networks. *J Biomed Mater Res* **1989,** *23* (10), 1183-1193, DOI: 10.1002/jbm.820231007.
(45) Fänger, C.; Wack, H.; Ulbricht, M., Macroporous poly(*N*-isopropylacrylamide) hydrogels with adjustable size "cut-off" for the efficient and reversible immobilization of biomacromolecules. *Macromol Biosci* **2006,** *6* (6), 393-402, DOI: 10.1002/mabi.200600027.
(46) Liao, H.; Munoz-Pinto, D.; Qu, X.; Hou, Y.; Grunlan, M. A.; Hahn, M. S., Influence of hydrogel mechanical properties and mesh size on vocal fold fibroblast extracellular matrix production and phenotype. *Acta Biomater* **2008,** *4* (5), 1161-1171, DOI: 10.1016/j.actbio.2008.04.013.
(47) Horn, J.; Hwang, W.; Jessen, S. L.; Keller, B. K.; Miller, M. W.; Tuzun, E.; Hartman, J.; Clubb, F. J.; Maitland, D. J., Comparison of shape memory polymer foam versus bare metal coil

treatments in an in vivo porcine sidewall aneurysm model. *J Biomed Mater Res B* **2017,** *105* (7), 1892-1905, DOI: 10.1002/jbm.b.33725.
(48) Armstrong, J. K.; Wenby, R. B.; Meiselman, H. J.; Fisher, T. C., The hydrodynamic radii of macromolecules and their effect on red blood cell aggregation. *Biophysical Journal* **2004,** *87* (6), 4259-4270, DOI: 10.1529/biophysj.104.047746.
(49) Khalil, E.; Kretsos, K.; Kasting, G. B., Glucose partition coefficient and diffusivity in the lower skin layers. *Pharm Res* **2006,** *23* (6), 1227-1234, DOI: 10.1007/s11095-006-0141-9.
(50) Kort, W. J.; Hekking-Weijma, J. M.; Tenkate, M. T.; Sorm, V.; VanStrik, R., A microchip implant system as a method to determine body temperature of terminally ill rats and mice. *Lab Anim* **1998,** *32* (3), 260-269, DOI: 10.1258/002367798780559329.
(51) Braverman, I. M., The cutaneous microcirculation. *J Investig Dermatol Symp Proc* **2000,** *5* (1), 3-9, DOI: 10.1046/j.1087-0024.2000.00010.x.
(52) Frost, M.; Meyerhoff, M. E., *In vivo* chemical sensors: tackling biocompatibility. *Anal Chem* **2006,** *78* (21), 7370-7377, DOI: 10.1021/ac069475k.
(53) Bryers, J. D.; Giachelli, C. M.; Ratner, B. D., Engineering biomaterials to integrate and heal: The biocompatibility paradigm shifts. *Biotechnol Bioeng* **2012,** *109* (8), 1898-1911, DOI: 10.1002/bit.24559.
(54) Anderson, J. M., Biological responses to materials. *Annu Rev Mater Res* **2001,** *31* (1), 81-110, DOI: 10.1146/annurev.matsci.31.1.81.

For Table of Contents Use Only

Foreign Body Reaction to a Subcutaneously Implanted Self-Cleaning, Thermoresponsive Hydrogel Membrane for Glucose Biosensors

*Alexander A. Abraham,‡ A. Kristen Means,‡ Fred J. Clubb, Jr., Ruochong Fei, Andrea K. Locke, Erica G. Gacasan, Gerard L. Coté, and Melissa A. Grunlan**